Characterization of the ice-binding protein from Arctic yeast *Leucosporidium* sp. AY30 ☆

Kyoung Sun Park [a,b,1], Hackwon Do [a,b,1], Jun Hyuck Lee [a,b,1], Seung Il Park [c], Eun jung Kim [a], Soon-Jong Kim [d], Sung-Ho Kang [a,b], Hak Jun Kim [a,b,*]

[a] *Division of Polar Life Sciences, Korea Polar Research Institute, Incheon 406-840, Republic of Korea*
[b] *Department of Polar Sciences, University of Science and Technology, Incheon 406-840, Republic of Korea*
[c] *Korea Ocean Research and Development Institute, Ansan 426-744, Republic of Korea*
[d] *Department of Chemistry, Mokpo National University, Chonam 534-729, Republic of Korea*

ABSTRACT

Previously, we reported the ice-binding protein (LeIBP) from the Arctic yeast *Leucosporidium* sp. AY30. In this study we provide physicochemical characterization of this IBP, which belongs to a class of IBPs that exhibited no significant similarity in primary structure to other known antifreeze proteins (AFPs). We compared native, glycosylated and non-glycosylated recombinant LeIBPs. Interestingly, size-exclusion chromatography and analytical ultracentrifugation revealed that LeIBP self-associates with a reversible dimer with K_d values in the range $3.45–7.24 \times 10^{-6}$ M. Circular dichroism (CD) spectra showed that LeIBP, glycosylated or non-glycosylated, is predominantly composed of β-strand secondary structural elements (54.6%), similar to other β-helical antifreeze proteins (AFPs). In thermal hysteresis (TH) activity measurements, native LeIBP was twice more active (0.87 °C at 15 mg/mL) than that of the recombinant IBPs (0.43–0.42 °C at 10.8 mg/mL). This discrepancy is probably due to uncharacterized enhancing factors carried over during ice affinity purification, because glycosylated and non-glycosylated recombinant proteins displayed similarly low activity. Ice recrystallization inhibition (RI) activities of the native and recombinant LeIBPs were comparable. Measurements of CD, TH activity, and RI showed that glycosylation does not cause structural changes and is not required for function. An ice-etching experiment using green fluorescent protein-tagged IBP revealed that LeIBP binds, just as hyperactive AFPs, to both basal and pyramidal prism planes of the ice crystal. Taken together, our results indicate that LeIBP, structurally similar to hyperactive AFPs, is moderately active and that a reversible dimer has no effect on its activity.

© 2012 Elsevier Inc. All rights reserved.

Introduction

Antifreeze proteins (AFPs) are generally characterized by two activities: thermal hysteresis (TH) activity, which is the difference between the freezing and melting points caused by inhibiting the growth of ice crystals in an AFP-containing solution and ice recrystallization inhibition (RI), which inhibits the growth of large grains of ice at the expense of smaller ones [9,14,12,27]. Ice-binding proteins (IBPs) were originally used to describe sea ice diatom proteins whose physiological function is probably to protect diatoms in brine channels between sea ice crystals without being damaged by freezing, instead of preventing bulk freezing of sea water [26]. But its present, broader use is to include any protein that binds to ice. This includes antifreeze proteins, proteins that inhibit ice recrystallization, proteins that anchor something to ice, and possibly even ice nucleation protein. Therefore, IBP provides a practical definition that includes both of these two functions – and potentially others – that require interaction with ice.

To date, AFPs or IBPs have been isolated from a wide variety of organisms, including fish [15], plants [58,54,23,60], bacteria [48,29,17,28], fungi [24], and insects [55,20,56,10,13,19]. A large number of biochemical and structural studies have been performed in order to understand the ice-binding mechanism at the molecular level. Strikingly, a large body of evidence shows that common functional properties of AFPs and IBPs can be accomplished by structurally diverse AFPs and IBPs [16,58,22,53]. A relatively recently identified class of IBPs or AFPs represented by the *Typhula ishikariensis* AFP (TiAFP) also confirmed this feature [26,32,57,4,5]. According to recent reports [57,5,61], this class of IBPs/AFPs had moderate to hyper TH activity but ice-binding

motifs of these proteins could not be searched for at the amino acid sequence level, exhibiting no significant similarity in primary structure to other known AFPs. Analysis of the amino acid composition and secondary structure prediction revealed that IBPs in this class contained a relatively high content of Ala, Gly, Ser, and Thr, and rare presence of Cys, and are mainly composed of β strand elements similar to other hyperactive AFPs [5,61,36]. However, unlike other β-helical AFPs that have abundant Thr residues, which usually form a Thr-X-Thr ice-binding motif on the outer surface of the β strand, they do not have a distinct repeating motif or sequence. Xiao et al. [61] reported that a recombinant version of the TiAFP isoform 8 showed high TH activity (approximately 2 °C) with RI activity, while wild type TiAFPs displayed moderate TH activity. The TH activity of the *Fragilariopsis cylindrus* AFP in the same class of protein was also moderate and hyperactive [57,5]. These examined proteins showed the explosive growth of ice crystal in a dendritic pattern with hexagonal symmetry at the end-point of the TH gap, called burst pattern, similar to those of hyperactive AFPs [20,18]. This implies that they may bind to basal planes as well as prism planes. But not all AFPs that bind to the basal plane of ice are hyperactive, although all hyperactive AFPs have affinity for the basal plane of ice. Currently, many IBPs in this class have been reported from the Antarctic sea ice diatom [26] and bacterium [48], Antarctic green alga [50], bacteria from the Vostok ice core [49], and mushrooms [47], but still little is known about this class of IBPs.

Recently, we have reported the extracellular ice-binding glycoprotein (LeIBP) from Arctic yeast *Leucosporidium* sp. AY30 belonging to the same class of TiAFP and demonstrated its antifreeze activity [36]. LeIBP consists of 261 amino acids and has a N-terminal signal sequence and one putative N-glycosylation site. We cloned, expressed and crystallized recombinant LeIBPs for further structure determination [46]. Here, we report the characterization of native LeIBP, and glycosylated/non-glycosylated recombinant LeIBPs in terms of their TH and RI activities, oligomerization, and ice-binding specificity for different ice crystal planes.

Materials and methods

Cloning, expression, and purification of LeIBP

For the characterization of LeIBP, heterologous protein was expressed in *Escherichia coli* and methylotrophic *Pichia pastoris*. To this end, the expression vectors were designed for four different protein constructs: bacterial LeIBP (bLeIBP), hexahistidine-tagged bacterial LeIBP (His-bLeIBP), enhanced green fluorescent protein (EGFP)-fused LeIBP (GFP-LeIBP), and *Pichia* LeIBP (pLeIBP).

The plasmid containing full-length cDNA of LeIBP was used as a template for the construction of the bacterial expression plasmids. The coding region of mature IBP cDNA was amplified by PCR using *Pfu* polymerase with the forward primer, 5′-CATA-TGCAGCGCGACCTCTCCGT containing an NdeI site, and the reverse primer, 5′-TCTAGATTAAAGCCACTGGCG containing an XbaI site. After A-tailing using Taq polymerase, the PCR product was cloned into the TOPO TA cloning vector (Invitrogen, USA). The insert was digested with NdeI and XbaI and ligated to pCold I and pCold IV expression vectors (Takara, Otsu, Shiga, Japan). The resulting plasmids were designated as pHis-bLeIBP and pbLeIBP, respectively.

The His-bLeIBP was expressed from *E. coli* BL21(DE3) harboring pHis-bLeIBP and purified as described elsewhere [46]. The bLeIBP was expressed and purified using ice affinity purification. To construct the GFP-LeIBP expression vector, a gene of enhanced green fluorescent protein (EGFP) was amplified from pIRES2-EGFP (Clontech, USA) using the forward primer 5′-GCAA CAT ATG GTG AGC AAG GGC G-3′ and the reverse primer 5′-GCAT GGT ACC ACC

AGA ACC ACC CTT GTA CAG CTC G-3′ containing a flexible linker (Ala-Ala-Gly-Ala) and inserted into the pCold I vector (Takara, Japan). The native LeIBP gene was amplified and cloned into the pCold I-GFP fusion vector digested with KpnI and BamHI. The resulting plasmid expresses a hexahistidine tag-GFP-LeIBP fusion protein.

For the production of N-glycosylated LeIBP (pLeIBP), the codon-optimized mature IBP gene was synthesized and cloned into a yeast pPICZαA expression vector (Invitrogen, USA) digested with XhoI and NotI. The vector harboring LeIBP gene was linearized by NotI and purified for transformation. Transformation of the *P. pastoris* X33 strain was performed using the electroporation method according to the manufacturer's instructions for the Multi-copy *Pichia* Expression Kit (Invitrogen Co., CA, USA). Selected *P. pastoris* transformants were cultured in 24 mL of BMGY (Buffered Glycerol-complex Medium, 1% yeast extract, 2% peptone, 100 mM potassium phosphate, pH 6.0, 1.34% YNB, 4×10^{-5}% biotin and 1% glycerol) medium with zeocin (100 μg/mL). Cells were grown at 30 °C with agitation until the OD_{600} reached 2.0. Cells were harvested by centrifugation at 3000g for 5 min at room temperature. Then, the cell pellet was resuspended in 1 L of BMMY (Buffered Methanol-complex Medium, 1% yeast extract, 2% peptone, 100 mM potassium phosphate, pH 6.0, 1.34% YNB, 4×10^{-5}% biotin and 0.5% methanol) medium and incubated at 28 °C. Methanol (0.5%, v/v) was added to the culture flask every 24 h in order to induce pLeIBP expression. After 48 h, culture media containing pLeIBP was separated by centrifugation at 13,000 rpm, for 10 min, at 4 °C. The supernatant was subjected to the ice affinity method [33].

The native LeIBP was purified from the culture medium as described previously [36]. Briefly, *Leucosporidium* sp. was grown in 3 L of Nutrient Broth at 4 °C for 7 days. The culture supernatant was clarified by centrifugation (8000 rpm for 30 min at 4 °C). Native IBP was purified using the ice affinity method [33] from the supernatant or 10× concentrated supernatant that was prepared using Tangential Flow filtration equipped with a 5000 MW cut off. The ice fraction was melted and concentrated by ultrafiltration (Millipore, MA, USA).

The bacterial version of LeIBPs, bLeIBP, His-bLeIBP and GFP-LeIBP were overexpressed in *E. coli* BL21 (Novagen, USA) transformed with appropriate expression vectors. The *E. coli* transformants were grown in a Luria–Bertani (LB) medium supplemented with ampicillin (50 μg/mL) and cultured at 37 °C overnight with agitation. One milliliter of the seed culture was transferred into 1 L of LB broth containing ampicillin (50 μg/mL) and cultured at 37 °C until the OD_{600} reached 0.5. Then, the culture media were placed at 15 °C and further incubated for 1 h. The recombinant IBPs were induced by adding isopropyl beta-D-thiogalactopyranoside (IPTG) to a final concentration of 1 mM and the cells were further cultivated at 15 °C for 15–20 h with agitation. The cells were harvested and stored at −70 °C until use.

The bLeIBP overexpressed bacterial pellet was suspended in 20 mM Tris HCl, pH 7.5, 100 mM NaCl and 0.1 mM EDTA and lysed using sonication. The lysate was clarified by centrifugation (12000 rpm for 1 h at 4 °C) and the bLeIBP was purified using ice affinity purification as described elsewhere [33].

The His-bLeIBP over expressed bacterial pellet was lysed in 20 mM KPi pH 7.4, 500 mM NaCl and 5 mM imidazole using sonication. The lysate was clarified by centrifugation (12000 rpm for 1 h at 4 °C) and loaded onto a Ni–NTA agarose column pre-equilibrated with a lysis buffer. The column was washed three times with one bed volume of washing buffer (20 mM KPi pH 7.4, 500 mM NaCl and 60 mM imidazole). The protein was eluted with a 500 mM imidazole gradient. The fractions containing the bLeIBP protein were pooled and dialyzed against a lysis buffer. Factor-Xa protease was added to the dialyzed material at a 1:50 M ratio

(for cleaving the hexahistidine tag) and the cleavage reaction was allowed to proceed overnight at 4 °C. The bLeIBP was further purified with a Superdex 200 size-exclusion column (Amersham Pharmacia). Fractions that showed >95% pure bLeIBP based on SDS–PAGE analyses were pooled. The concentrations of bLeIBP were determined using UV spectrophotometry with an extinction coefficient at 280 nm of 26,930 M^{-1} cm^{-1} based on the amino acid sequence.

GFP-LeIBP was also purified as described above with an additional ice affinity purification step added after Ni-affinity chromatography.

Polyacrylamide gel electrophoresis, immunoblotting, N-terminal sequencing

Sodium dodecyl sulfate–polyacrylamide gel electrophoresis (SDS–PAGE) was conducted with a Mini-PROTEAN II electrophoresis cell unit (BioRad) as described previously by Laemmli [34]. Protein samples were boiled for 10 min at 95 °C in the protein sample buffer, and after electrophoresis, the protein band was visualized with Coomassie brilliant blue R250 or silver staining.

To stain glycoproteins using Periodic acid Schiff reagent (PAS) staining, the SDS–PAGE gel was immersed in a 40% ethanol, 7% acetic acid solution for 1 h, washed with distilled water for 1 min, transferred to a 1% periodic acid solution containing 3% acid acetate, and kept for 1 h. Then, it was washed thoroughly with distilled water to remove the periodic acid, followed by incubation in a Schiff reagent solution in the dark for 1 h. Finally, staining was terminated by incubating the gel in 0.58% potassium metabisulfite and a 3% acetic acid solution. Western blotting was carried out using an antibody raised against His-bLeIBP as described elsewhere [52].

Purified native LeIBP, pLeIBP, bLeIBP were electrophoretically transferred to a PVDF membrane, immediately following SDS–PAGE. The membrane was rinsed three times with distilled water and stained with Ponceau S. The bands corresponding to LeIBPs were excised and subjected to N-terminal amino acid sequencing using Edman degradation with a 491 Procise amino acid Sequencer (Applied Biosystems, Foster city, CA, USA) at the Korea Basic Science Institute (Ochang, Korea).

Size-exclusion chromatography

The molecular mass of the purified LeIBPs was estimated by size-exclusion chromatography using a TSK-G2000SWxl column (Tosoh Bioscience, Tokyo, Japan). The column, connected to a YL9100HPLC system (Young Lin Instruments Co., Ltd., Anyang, Korea), was equilibrated with 2 column volumes of 20 mM Tris–HCl, pH 8.0 and 150 mM NaCl at a flow rate of 1 mL/min at 22 °C. The column was calibrated with bovine serum albumin (66 kDa), carbonic anhydrase (29 kDa), cytochrome C (12.4 kDa), and aprotinin (6.5 kDa). The calibration curve was generated by plotting the partition coefficients (K_{av}) of standard proteins versus the logarithm of their molecular mass. K_{av} was calculated from the equation:

$$K_{av} = (V_e - V_o)/(V_t - V_o),$$

where V_e is the peak elution volume, V_o is the void volume, which was determined using blue dextran, and V_t is the total bed volume of the column. Twenty microliter of a 1 mg/mL of native LeIBP, pLeIBP, and His-bLeIBP solution was injected into the column and eluted with the same buffer. The elution volumes were used to calculate the K_{av} values of LeIBPs and their molecular mass was determined from the calibration curve. Eluted fractions were further analyzed by SDS–PAGE to confirm the presence of LeIBPs.

Equilibrium sedimentation

Equilibrium sedimentation studies were performed using a Beckman ProteomeLab XL-A analytical ultracentrifuge in a 20 mM Tris–HCl buffer, pH 8.0, containing 150 mM NaCl at 20 °C. LeIBP samples were measured at 280 nm using two-sector and six-sector cells at rotor speeds of 18,000, 20,000 and 24,000 rpm to check reversibility. All measured data fit well to a reversible monomer (1x)–dimer (2x) equilibrium model and representative results measured at 20,000 rpm (native LeIBP) and 24,000 rpm (His-bLeIBP) using ca. 63 and 93 μM protein are presented. The concentration of LeIBPs was calculated using $e_{280\ nm} = 26930\ M^{-1}\ cm^{-1}$ and molecular weights of 24925 and 27082 Da for native LeIBP and His-bLeIBP, respectively, calculated from their amino acid compositions. Since the native and P. pastoris expressed LeIBPs are glycosylated (approximately 2.5–5%, unpublished results), 3% glycosylation was assumed in the fitting processes. For His-bLeIBP, no glycosylation was considered. The time required for the attainment of equilibrium was established by running at the given rotor speed until the scans were invariant for 4 h: this was achieved, at most, after 48 and 72 h in the six- and two-sector cells, respectively. Partial specific volume of the protein and buffer density were calculated using the software Sednterp [35]. The calculated partial specific volume at 20 °C was 0.7348 cm^3/g and the buffer density was 1.00499 g/cm^3. For data analysis by mathematical modeling using non-linear least-squares curve fitting, fitting functions were used for His-bLeIBP (Eqs. (1) and (3)) and native LeIBP and pLeIBP (Eqs. (2) and (4)). Eqs. (1) and (2) represent homogeneous models and Eqs. (3) and (4) represent a reversible 1x–2x model.

$$C_r = C_b \exp(A_p M_p(r^2 - r_b^2)) + \varepsilon \tag{1}$$

$$C_r = C_b \exp((A_p M_p + A_c M_c)(r^2 - r_b^2)) + \varepsilon \tag{2}$$

$$C_r = C_b \exp(A_p M_p(r^2 - r_b^2)) + C_b^2 \exp(ln K_a + A_p M_p(r^2 - r_b^2)) + \varepsilon \tag{3}$$

$$C_r = C_b \exp((A_p M_p + A_c M_c)(r^2 - r_b^2)) + C_b^2 \exp(ln K_a + (A_p M_p + A_c M_c)(r^2 - r_b^2)) + \varepsilon \tag{4}$$

$$A_i = (1 - v\rho)w^2/2RT$$

In the above equations, C_r is the total concentration at the radial position r, C_b is the concentration of protein at the bottom of the cell, and M_p and M_c are the molecular weights of protein and carbohydrate (3% and 750 Da), respectively. The partial specific volume and the solution density are demoted by v and ρ, respectively. A partial specific volume value of 0.63 cm^3/g was used for the carbohydrate. The rotor angular velocity is denoted by w, and a baseline error term, by ε. The $ln\ k_a$ values are natural logs of the equilibrium constants of the reversible 1x–2x association on an absorbance scale and must be converted to a molar scale for thermodynamic calculations. These are given by $ln\ K_a = ln\ k_a + ln(e_1/2)$, where e_1 (for LeIBP, $26,930 \times 1.2 = 32,316\ M^{-1}\ cm^{-1}$) is a corrected extinction coefficient of the LeIBP monomer at 280 nm; the multiplicative value of 1.2 was used because the optical path length of the XL-A cells are 1.2 cm rather than 1.0 cm. The model was selected by examining the weighted sum of square values, and weighted root mean square error (RMSE) values. Further data manipulation and data analysis by mathematical modeling were performed using MATLAB [31] operating on a data analysis computer.

Circular dichroism spectroscopy

Circular dichroism (CD) measurements were performed using a Chirascan CD spectrometer (Applied photophysics Co., UK) with a Peltier temperature controller. Samples were placed in either 1 or 10 mm path length quartz cuvettes (Hellma, USA). Spectra were collected from 190 to 260 nm for far-UV CD and from 250 to 350 nm for near-UV CD at 20 °C and with a 1 nm bandwidth. Ten spectra were averaged to give the final trace, and buffer spectra were subtracted. Protein concentrations were 40 μM in distilled water for both the far- (1 mm cell) and near-UV (10 mm cell) CD measurements. The secondary structures were estimated from CD spectra using interactive circular dichroism analysis software CDNN [6]. CD results were expressed as mean residue ellipticity, given in mdeg cm^2 dmol^{-1}.

Thermal hysteresis activity and ice re-crystallization inhibition assay

Thermal hysteresis was measured using a nanoliter osmometer (Otago Osmometers, Dunedin, New Zealand) connected to a cold well stage mounted on a light microscope equipped with a Canon Digital Camera and the effect on ice crystal morphology was recorded. The sample was placed on a sample well on the cold stage and frozen rapidly at around −20 °C. To obtain a single ice crystal, the temperature was raised slowly. When the ice crystal morphology was maintained, the temperature was lowered again slowly (−0.04 °C/min). The freezing point of the sample was determined as the temperature at which the rapid growth of the ice crystal was observed. The maximum difference between the annealing temperature and the freezing point during the slow cooling steps was used as an approximation to the sample's freezing point depression activity. Samples were prepared in distilled water and concentration of the proteins ranged from 0 to 17.75 mg/mL.

Ice recrystallization inhibition (RI) activity was measured using an equal volume mixture of a 60% sucrose solution and purified LeIBPs by the Smallwood method [54] using a Linkam TMHS600 cold stage (Linkam Scientific Instruments, Surrey, UK) mounted with an Olympus BX51 upright microscope. Four microliter of the sample solution was sandwiched between two circular 16 mm-diameter cover slips. The sandwich was pre-chilled to prevent frost on the surface at −1 °C. After 3 min, the sandwich was transferred to a circulating cooling stage. The temperature was quickly lowered to −80 °C at a rate of 90 °C/min, and maintained for 1 min. The sandwich was then warmed to −6 °C for 60 min to allow for ice re-crystallization to occur. Thereafter the sandwich was viewed using a microscope (Olympus) and images captured every 5 min.

Ice-etching experiment

Single ice crystal preparation and an ice-etching experiment were performed using the method of Knight et al. [30] with a slight modification. A single ice crystal was confirmed by viewing it under polarizing filters. In addition, a control experiment with Type III AFP produced the same result as previously reported [3] (data not shown), confirming that the hemispheres were single crystals. A single ice crystal (2.5 cm × 2.5 cm × 2.5 cm) was mounted with two different orientations: one with the basal plane normal to the long axis of the cold-finger, and the other with the primary prism plane normal to the long axis of the cold-finger. Then the single ice crystal mounted on the cold-finger was immersed into degassed water (4 °C). Then, the temperature of the coolant was lowered to −7 °C and the ice crystal was grown into the ice hemisphere for 3–4 h. The ice hemisphere was then dipped into a protein solution (1–5 μM) and the temperature was lowered to −10 °C. After 30 min, the ice hemisphere was removed from the

cold-finger and transferred to a cold room at −15 °C. The surface of the ice hemisphere was scraped using a sharp blade and then left to evaporate, to obtain a distinct etching pattern. The proteins used in this experiment were native LeIBP, pLeIBP, His-bLeIBP and GFP-LeIBP. Bound GFP-LeIBPs were excited using 460–500 nm light and the emission was photographed.

Results

Preparation of native and recombinant LeIBPs

To characterize the LeIBP, the recombinant proteins were expressed in two different hosts. The effect of glycosylation on the activity of LeIBP was also investigated using glycosylated and non-glycosylated recombinant LeIBPs. Fig. 1 summarizes the recombinant protein constructs, SDS–PAGE, and PAS staining of purified proteins. The native LeIBP was purified from either concentrated or non-concentrated culture media using ice affinity chromatography. During the ice affinity purification from the concentrated culture media, we noticed that the ice-binding fraction contained brownish substances, which seemed to be mainly polysaccharides (unpublished data). These impurities were not completely eliminated after a few rounds of ice affinity purification and buffer exchange steps using ultrafiltration. The sample preparation of native LeIBP was varied from batch to batch. We were able to eliminate more of the impurities by starting with non-concentrated culture supernatant. In this study, we used two native LeIBP samples: one was a brownish and slightly viscous sample purified from the concentrated culture media, designated native LeIBP A, and the other was a slightly yellowish sample from non-concentrated media, designated native LeIBP B. Since TH activity stemmed solely from LeIBP, as previously described [36], we attempted to characterize LeIBP. This paper focuses on the IBP instead of the TH enhancer. The total amounts of native LeIBP A and B purified from a 1 L culture were 2.4 and 10.3 mg, respectively.

The cDNA sequence of LeIBP has previously been reported [36]. The nucleotide sequence encoding the mature IBP without the signal peptide (20 residues) was amplified and cloned into bacterial pCold expression vectors (Fig. 1). Three bacterial recombinant LeIBPs (bLeIBP, His-bLeIBP, and GFP-LeIBP) were overexpressed under the control of the promoter of the cold shock protein A (cspA) gene in *E. coli*. The expressed His-bLeIBP has an additional 17 amino acids consisting of a translation-enhancing element (TEE), a hexahistidine tag, and a Factor Xa cleavage site, while only a Met codon was added to bLeIBP for translation initiation. The overexpressed IBPs were located in both the soluble and insoluble fractions. However, because the soluble fractions contained enough IBPs (more than 50% of the total expressed protein), IBPs were purified from the soluble fractions. Ni(II)-NTA-based metal ion chelate chromatography was employed to purify His-bLeIBP and GFP-LeIBP. Ice affinity chromatography was used for the final purification of GFP-LeIBP or to purify bLeIBP with no affinity tag.

Because native LeIBP is glycosylated [36] and because bacterially-expressed proteins are non-glycosylated, we attempted to express glycosylated LeIBP in a *Pichia* yeast expression system. The coding sequence was optimized and ligated to pPICZαA. *P. pastoris* X33 cells transformed with the pLeIBP plasmid secreted the mature LeIBP when cultured in the presence of 0.5% methanol. The culture supernatant containing secreted pLeIBP was harvested and concentrated 10 times using tangential flow filtration with a 10 kDa molecular weight cut-off membrane. The concentrate was subjected to ice affinity chromatography as described above. The ice fractions were melted and concentrated using a Centricon 10 K centrifugal filter (Millipore, MA, USA).
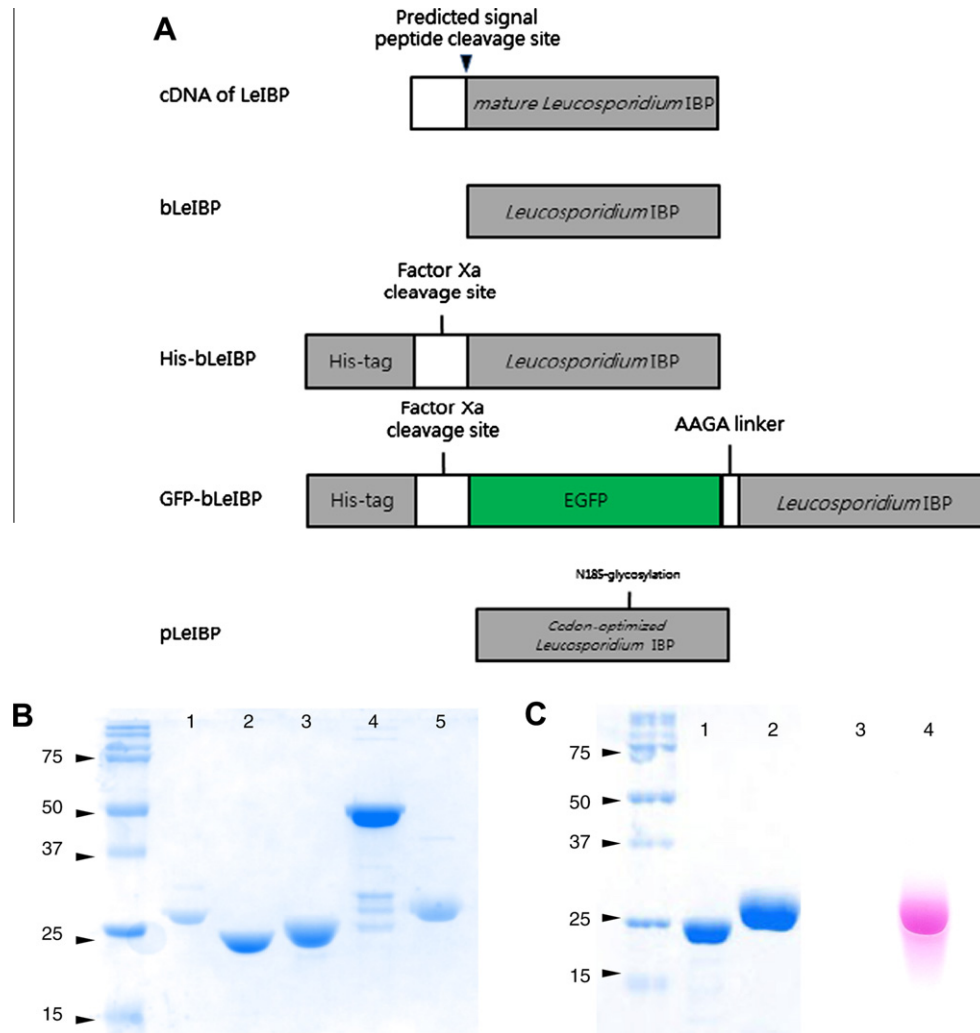
Fig. 1. Cloning, expression, and purification of native and recombinant LeIBPs. (A) Schematic diagram of four different recombinant LeIBPs (bLeIBP, His-bLeIBP, GFP-LeIBP, pLeIBP). (B) SDS–PAGE analysis of purified native LeIBP (lane 1), bLeIBP (lane 2), His-bLeIBP (lane 3), GFP-IBP (lane 4) and pLeIBP (lane 5). (C) Coomassie brilliant blue staining of His-bLeIBP (lane 1), pLeIBP (lane 2) and PAS staining of His-bLeIBP (lane 3), pLeIBP (lane 4). Hexa histidine-tagged bacterial LeIBP (His-bLeIBP) did not show any bands in PAS staining.

The yields of purified protein from a 1 L culture medium were 2.1 mg for bLeIBP, 24.5 mg for His-bLeIBP, 19.3 mg for GFP-LeIBP, and 61.2 mg for pLeIBP. The calculated molecular weights of bLeIBP, His-bLeIBP, GFP-LeIBP, and pLeIBP are 25057, 27082, 54290, and 24925 Da, respectively. SDS–PAGE of purified LeIBPs (Fig. 1B) revealed a single band with a relative molecular weight corresponding to their molecular weight calculated from their primary structure. However, native and *Pichia* LeIBP migrated slower than bLeIBP (non-glycosylated LeIBP), probably as a result of glycosylation at the potential N-glycosylation site (Asn185). In addition, PAS staining revealed a 27 kDa band, whereas no PAS-stained band was found with bacterially-expressed bLeIBP (Fig. 1C). Digestion of pLeIBP of N-linked glycans with peptide N-glycosidase F (PNGase F), which removes N-linked glycans, reduced the molecular weight by approximately 2 kDa, observed with SDS–PAGE, to the expected value for bLeIBP (∼24.9 kDa), and resulted in no PAS staining. This implies that pLeIBP, similar to native LeIBP, is expressed in the N-glycosylated form (data not shown). Except for GFP-LeIBP, the purity of the protein was estimated to be ⩾95%.

The N-terminal amino acid sequencing of pLeIBP and bLeIBP revealed the first few amino acids as QRDLS and MQRDLSVELG, which correspond to the N-terminus of the mature IBP, clearly demonstrating that the recombinant proteins were correctly trans-lated. However, a few attempts to obtain the N-terminal sequence of native LeIBP were unsuccessful. Western blot analysis using an antibody raised against bLeIBP also confirmed that the purified proteins were LeIBPs (data not shown).

Oligomeric state of LeIBPs

To determine the molecular weight and the oligomeric state of LeIBPs in solution we performed size-exclusion chromatography and equilibrium sedimentation. Analysis by size-exclusion chromatography was carried out by HPLC using a TSK-G2000SWxl column. A linear plot of K_{av} versus $\log M_r$ was derived from the elution profiles of a number of protein standards and was used to estimate the molecular weights of LeIBPs in solution. Based on the elution volume, the calculated molecular weights were approximately 39.7 kDa for native LeIBP, 41.8 and 47.2 kDa for the first and second peaks of pLeIBPs, and 45.3 kDa for His-bLeIBP (Fig. 2B). Except for the first peak of pLeIBP, the glycosylated LeIBPs (native LeIBP and pLeIBP) migrated slightly slower than non-glycosylated His-bLeIBPs whose monomer molecular weight is greater due to the 6X His and other linkers than those of the other two LeIBPs' monomers. Interestingly, these values are very close to the average of a monomer and a dimer. As shown in Fig. 2C, LeIBPs gave broad and
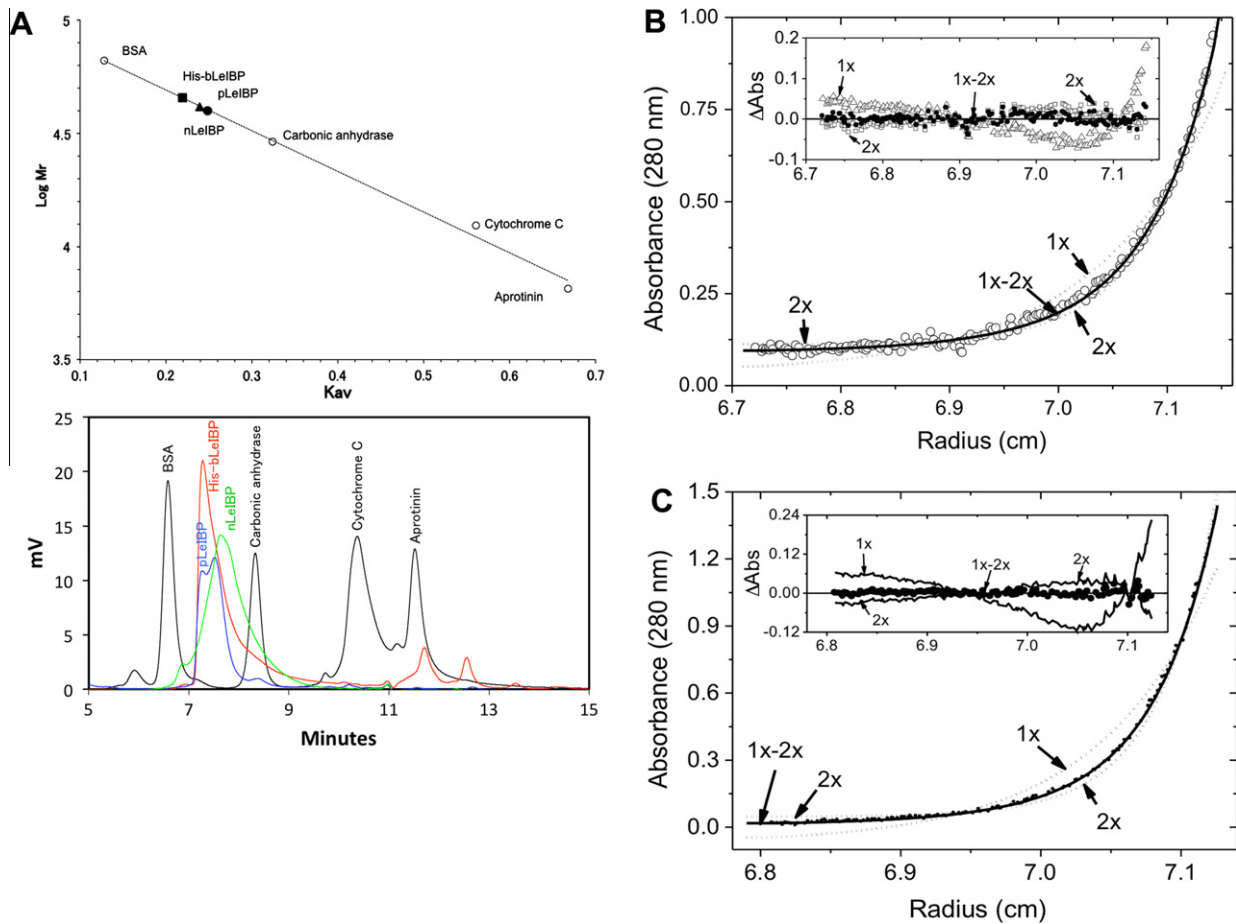
Fig. 2. Molecular weights and oligomeric states of LeIBPs. (A) (upper panel) Standard K_{av} versus log MW graph of LeIBPs using size-exclusion chromatography. (Lower panel) Elution profiles of LeIBPs compared with protein standards. His-bLeIBP (■, red) eluted first followed by pLeIBP (▲, blue) and native LeIBP (●, green). The molecular mass of the purified LeIBPs was estimated by size-exclusion chromatography using a TSK-G2000SWxl column equilibrated with 2 column volumes of 20 mM Tris–HCl, pH 8.0 and 150 mM NaCl at a flow rate of 1 mL/min at 22 °C. Protein standards were bovine serum albumin (66 kDa), carbonic anhydrase (29 kDa), cytochrome C (12.4 kDa), and aprotinin (6.5 kDa). The calibration curve was generated by plotting partition coefficients (K_{av}) of standard proteins versus the logarithm of their molecular mass. K_{av} was calculated from the equation described in Materials and methods. (B and C) Sedimentation equilibrium distribution (circle) of native LeIBP (B) and His-bLeIBP (C). The concentration of the protein was 93 μM (0.23 mg/mL). The circles are experimental results at 280 nm and the solid line is a fitting line for a reversible monomer (1x)–dimer (2x) equilibrium model. The dotted lines are fitting lines for ideal homogeneous 1x and 2x models. The calculated molecular mass for native LeIBP 1x from its amino acid composition is 24930 Da. For the fittings, 3% of glycosylation with a molecular mass of 750 Da and a partial specific volume of 0.63 g/cm^3 was used for the carbohydrate contribution. (Inset of 2B) Distributions of the residuals for the monomer (1x, triangle) and dimer (2x, square). The residuals for the reversible 1x–2x model are shown as filled circles. The random distributions of the residuals for the reversible 1x–2x model indicate that native IBP exists as equilibrium mixtures of 1x and 2x in solution. The homogeneous 2x model shows systematic deviations at both lower and higher radial positions. Sedimentation equilibrium distribution (filled small circles) of His-bLeIBP (C) protein in 20 mM Tris–HCl buffer, pH 8.0 containing 150 mM NaCl at 20,000 rpm and at 20 °C. The concentration of the protein was 93 μM (0.23 mg/mL). The small filled circles along with a solid line are experimental data at 280 nm and the solid line is a fitting line for a reversible monomer (1x)–dimer (2x) equilibrium model. The dotted lines are fitting lines for ideal homogeneous 1x and 2x models. Calculated molecular mass for bacterial IBP 1x is 25,194 Da. For the bacterial IBP, glycosylation was not considered. (Inset of 2C) Distributions of the residuals for the monomer (1x, solid line) and dimer (2x, solid line). The residuals for the reversible 1x–2x model are shown as filled circles. The random distributions of the residuals for the reversible 1x–2x model indicate that His-bLeIBP exists as equilibrium mixtures of 1x and 2x in solution. The homogeneous 2x model shows systematic deviations at both lower and higher radial positions.

tailing peaks while elution profiles of the protein standards were symmetric (Fig. 2B). Native LeIBP gave one major peak with a previously-eluted auxiliary peak. pLeIBP showed a split major peak with a smaller peak that eluted later around 29 kDa. His-bLeIBP gave only one major peak with minor peaks smaller than 6.5 kDa, which we assumed to be minor contaminants or proteolytic products. The tailing peak shape typically appears when dimers dominate owing to their intermediate association and dissociation with monomers. These data strongly indicate that LeIBP undergo an exchange between monomer and dimer in solution. Another possible explanation is that the shape of LeIBP may be elongated and the protein eluted earlier than expected. However, considering that AFPs and IBPs in this class seem to conform to the β-helical type structure model based on structure (data not shown), the shape of the protein is not elongated. It should also be
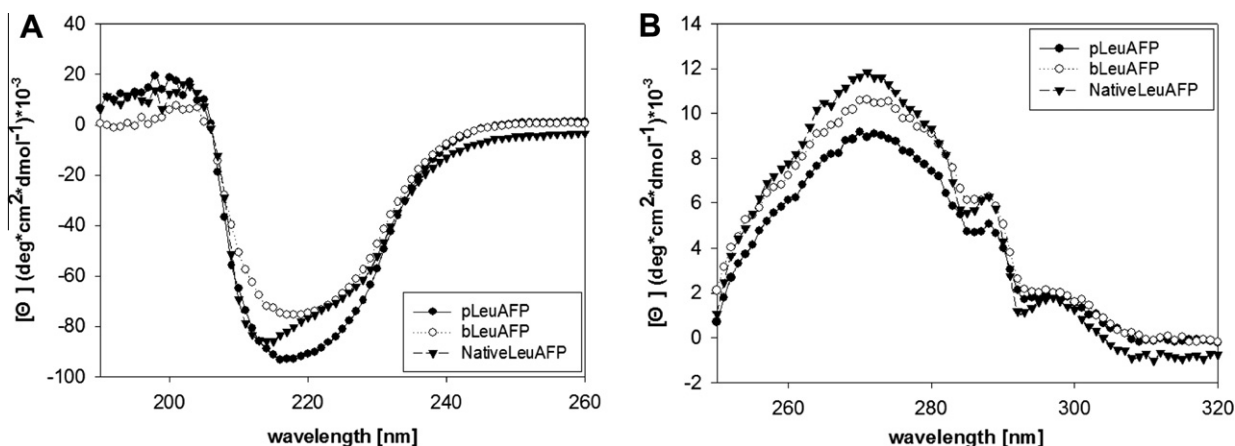
noted that, as shown in Fig. 2B, the peak profiles, which are broad for native IBP and split for pLeIBP, are likely due to the heterogeneity of the degrees of glycosylation in the purified proteins, which gave several split signals, the difference between which corresponds to the molecular weight of one hexose (data not shown).

We further investigated the oligomeric states using analytical ultracentrifugation techniques under various conditions and obtained the equilibrium constants of LeIBPs. These constants corresponded to the intermediate monomer–dimer exchange rate. Fig. 2C shows the data and fits for native LeIBP monomer (1x), dimer (2x) and 1x–2x reversible equilibrium models at an ultracentrifugal speed of 20,000 rpm. The weighted RMSEs for the 1x and 2x fits were 4.43×10^{-2} and 1.93×10^{-2}, respectively. The reversible 1x–2x equilibrium model gives a substantially improved RMSE value of 1.17×10^{-2}. In the inset of Fig. 2C, residual

plots are also shown. While the 1x–2x reversible model shows a random residual distribution, it is noticeable that the 2x model shows systematic deviation at the beginning and end of the radial positions. Equilibrium sedimentation data measured at different speeds (18000 and 24000 rpm) and different concentrations (63 and 93 μM) also support the reversible 1x–2x model. From the fitting process using Eq. (4), a $ln\ K_a$ value of 12.58 was obtained corresponding to a dissociation constant, $K_d = 3.45 \times 10^{-6}$ M. We further confirmed the reversible 1x–2x equilibrium using His-bLeIBP, which lacks glycosylation. In Fig. 2D, the sedimentation equilibrium analysis of His-bLeIBP at 24000 rpm is shown. The RMSE values for the 1x and 2x fits were 6.81×10^{-2} and 2.79×10^{-2}, respectively. The reversible 1x–2x equilibrium model gave a much improved RMSE value of 9.27×10^{-3} with a $ln\ K_a$ value of 11.85 corresponding to a dissociation constant, $K_d = 7.24 \times 10^{-6}$ M. A slightly higher K_d value for His-bLeIBP than that of native LeIBP probably originated from the difference in the glycosylation. In Fig. 2D inset, residual plots are shown. The 1x–2x reversible model also shows much better residual distribution. In this figure, residual plots for the 1x and 2x models shown in solid lines clearly indicate the inferiority of the homogeneous models (1x and 2x) as compared to the 1x–2x reversible equilibrium model. pLeIBP also showed similar behavior (1x–2x equilibrium) whose data are not presented here.

Circular dichroism of LeIBP

The far-UV CD spectra of the LeIBPs were very similar, with a strong negative minimum at 214–217 nm (Fig. 3A), indicating that the native and recombinant LeIBPs have almost identical secondary structures. An analysis of the spectra by CDNN estimated that LeIBP is predominantly composed of β-strands (67.4%) (Table 1), which is not surprising given that the IBPs belonging to this class showed a high propensity to have a β-strand as a secondary structure element [37,42,16]. The near-UV (250–320 nm) ellipticity (Fig. 3B) is largely due to aromatic amino acids in an asymmetric chemical environment of a protein, as well as disulfide bonds, and provides tertiary structural information. The near-UV CD spectra of all LeIBPs were also very similar, showing significant positive signals in the aromatic regions. These results clearly indicate that native and recombinant LeIBPs have similar well-folded tertiary structures. The 275 nm peak corresponds to 7 tyrosine residues and 11 phenylalanine residues, and the 288 nm peak corresponds to 3 tryptophan residues.

Table 1
Prediction of secondary structure composition of LeIBPs by CD and PSIRED.

Secondary structure elements	Far-UV CD			PSIPRED[a] (%)
	Native LeIBP (%)	pLeIBP (%)	His-bLeIBP (%)	
α-Helix	17.0	18.8	19.4	32.08
β-Strands	76.0	67.4	63.8	54.58
Random coil	42.9	42.2	42.6	13.33

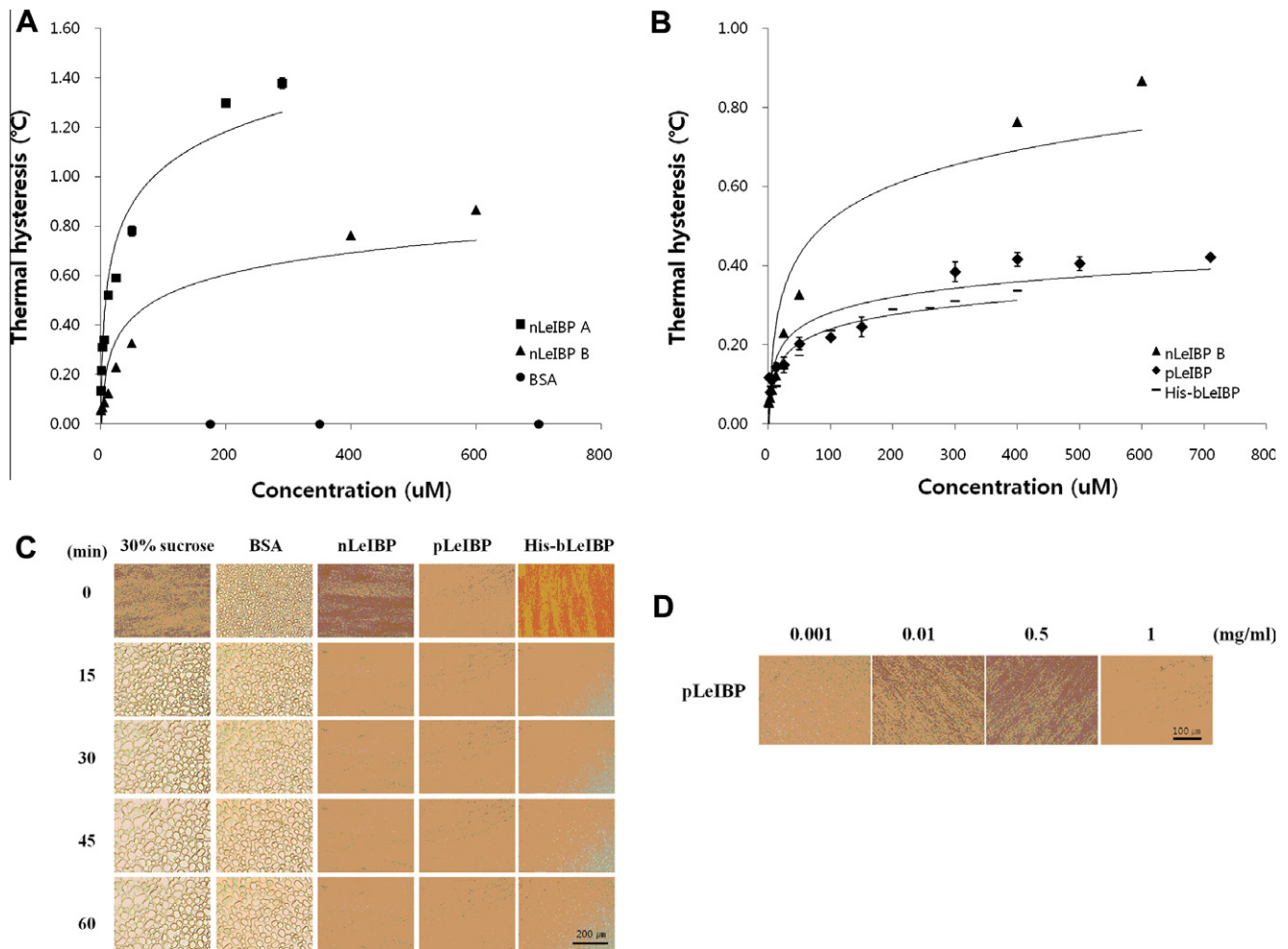[a] Secondary structure prediction from the PSIPRED web server.

TH and RI activities of LeIBPs

As stated above, ice affinity purification and a few rounds of ultrafiltration did not completely remove all impurities from the native LeIBP samples. When concentrated, the solution became more viscous and darker. The impurities seemed to include polysaccharides (data not shown). The composition of the impurities is currently under investigation. The TH of the impure LeIBP A (e.g., 1.38 °C at 7.25 mg/mL) was twice that of the less viscous and faint yellowish LeIBP B (e.g., 0.87 °C at 15 mg/mL) (Fig. 4A).

At concentrations of 400 μM (10 and 10.8 mg/mL of pLeIBP and His-bLeIBP, respectively), glycosylated pLeIBP and non-glycosylated His-bLeIBP had similar THs (0.42 °C and 0.34 °C, respectively) (Fig. 4B), suggesting that glycosylation is not required for TH. The TH activities of His-bLeIBP and bLeIBP were similar, hence in the following, all activity assays of the bacterial version of LeIBP were done with His-bLeIBP. For an unknown reason, the THs of the recombinant proteins were approximately half the TH of native LeIBP B (see Discussion). LeIBP, pLeIBP and His-bLeIBP all showed strong recrystallization inhibition activities (Fig. 4C), even though recombinant LeIBPs have a lower TH activity than native LeIBP. The minimal pLeIBP concentration displaying RI activity was 0.001 mg/mL (Fig. 4D).

Ice-etching experiment

The plane(s) of ice to which LeIBP binds were determined by the etching of single ice crystal hemispheres. To improve the visualization of the ice surface, we also used GFP-LeIBP that was almost as active as His-bLeIBP based on their TH activities. Since some AFPs bind to multiple ice planes [53,18,21,39,45], ice hemispheres with different crystallographic planes were mounted on a cold-finger to orient either the basal plane or the primary prism plane normal to

Fig. 3. Circular dichroism analysis of LeIBPs. (A) Far-UV spectra of native LeIBP, pLeIBP (●) and bLeIBP (○). (B) Near-UV spectra of native LeIBP, pLeIBP (●) and bLeIBP (○). The spectrum is the average of 10 measurements recorded at 20 °C with protein concentrations of 1 mg/mL. CD data were expressed as mean residue ellipticity θ, given in mdeg cm² dmol⁻¹.

Fig. 4. Antifreeze activity of LeIBPs. (A) Thermal hysteresis activity of native LeIBP A (■, brownish sample) and native LeIBP B (▲, clear sample) purified from culture supernatant was compared to BSA (●). (B) Comparison of the observed TH activity of native LeIBP B (▲), pLeIBP (♦) and His-bLeIBP (-). Measurements were carried out in triplicate as a function of concentration. (C) Recrystallization inhibition activity by purified native LeIBP, pLeIBP and His-bLeIBP (1 mg/mL) at −4 °C in 30% sucrose solution. Ice crystal images were collected every 5 min for 60 min. The scale bar represents 200 μm. (D) Concentration-dependent recrystallization inhibition activity of pLeIBP at 60 min. The pLeIBP concentration is 0.001, 0.01, 0.5, and 1 mg/mL. The scale bar represents 100 μm.

the finger. Native LeIBP etched the top of the hemisphere (Fig. 5A), indicating that it bound to the ice basal plane. However, a very faint etching pattern was observed on the prism faces. This was also the case for pLeIBP and His-bLeIBP.

In contrast to the above, the etching pattern was clearer with GFP-LeIBP, which preferentially bound to the primary prism planes (Fig. 5B). When the hemisphere was grown with the *c*-axis normal to the cold finger, it had strong fluorescent signals on the basal planes and weaker signals on the primary prism planes (Fig. 5C), so that the unbound areas on the ice surface corresponded to the secondary prism planes. These results indicate that LeIBP, just as hyperactive AFPs [20,18], binds to multiple ice planes, preferentially to the basal and primary prism planes.

Discussion

In the present study, we report the physicochemical characterization of the recently reported ∼25 kDa IBP from Arctic yeast, which shows 55% identity with TiAFP, a representative protein of less characterized class of IBPs or AFPs. Our results show that this IBP undergoes reversible dimerization, that it has a relatively low TH activity regardless of glycosylation, and that it binds to the basal and primary prism planes of the ice crystal.

LeIBP is a reversible dimer in solution

The oligomeric state of LeIBP, examined by two independent methods, was found to be a self-associated reversible dimer in solution. The monomer–dimer exchange rate is intermediate, as demonstrated by the tailing peak in size-exclusion chromatography and by the dissociation constant obtained using analytical ultracentrifugation. This implies that LeIBP coexists as a monomer/dimer pair but predominantly as a dimer in solution. These data are interesting in that this reversible dimerization has not been observed in other diatom and fungal AFPs belonging to the same class. Our recent effort in determining the structure of LeIBP revealed that the asymmetric unit of the protein crystal contains two molecules; a dimer is formed partly by C-terminal tail swapping (manuscript under review), which is consistent with the data described above. While many AFPs are monomeric, dimeric AFPs, or proteins with two AFP or IBP domains, have been occasionally reported [43,1,41,38,59,49]. The ∼17 kDa hyperactive fish Type I h is known to associate as a highly asymmetric dimer whose native molecular weight (∼66 kDa) is greater than the calculated molecular weight of a dimer (∼34 kDa). Smelt type II AFP, as shown in Figs. 5 and 6 from Achenbach and Ewart [1], formed a dimer in solution. In the gel-filtration analysis of smelt AFP, one major peak with a tail eluted at the molecular weight of a dimer. It would
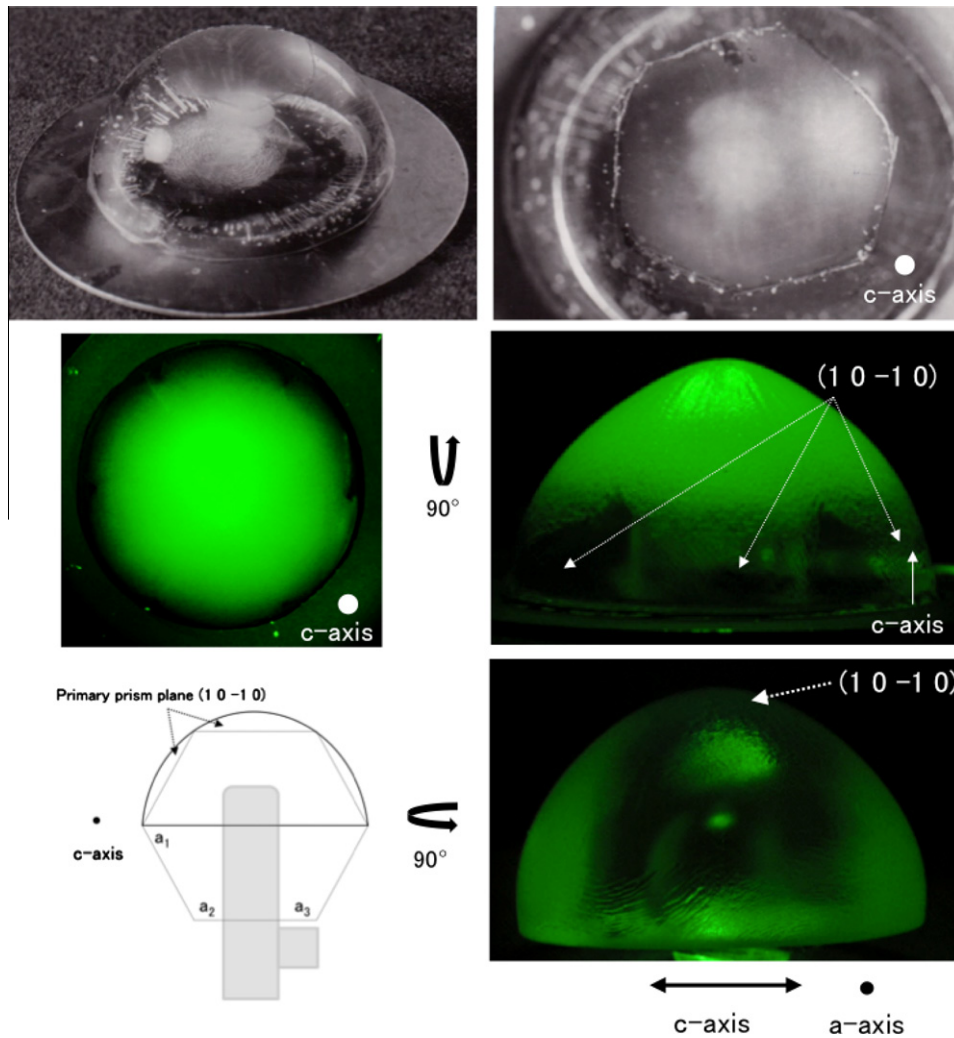
Fig. 5. Ice etching photographs of LeIBPs. (A, left) Single crystal hemispheres grown in native LeIBP-containing solution with the *c*-axis parallel to the cold-finger and (A, right) top view of hemisphere on the left. (B, left) Single ice crystal grown in 5 μM of GFP-LeIBP solution with its *c*-axis parallel to the cold-finger and (B, right) side view of the hemisphere on the left. Bound GFP-LeIBP was excited by a 460–500 nm light and emission was photographed through a 509 nm filter. (C, left) Schematic drawing of the hemisphere grown with its *c*-axis normal to the cold-finger and (C, right) the hemisphere grown in 5 μM of GFP-LeIBP solution with the same configuration on the left.

therefore seem that two AFPs have a stronger tendency to form a dimer than LeIBP.

β-Helical LeIBP is moderately active, not hyperactive

Dimerization or oligomerization seems to be beneficial in that TH activity tends to increase as the size of AFPs increases, which can often lead to the increase in the ice-binding area of AFPs [7]. In addition, TH activity can be affected by how ice-binding sites (IBS) are formed or aligned in the dimeric proteins. For example, the fish type I AFP isoforms whose size are one fifth of the type Ih AFP monomer and one tenth of the type Ih dimer shows one tenth to one hundredth TH activity of type Ih AFP dimer [44]. Contrarily smelt type II AFP has little effect on TH activity [2]. The LeIBP is likely to be the case of smelt AFP, which is supported by the fact that both native and recombinant LeIBPs, even at a higher concentration, showed a lower TH activity than moderate AFPs or IBPs in the same class. We speculate that this is probably because one IBS may point away from ice, while the other binds ice, decreasing the effective concentration of IBSs in the dimer.

Far-UV CD and X-ray crystal structure studies (manuscript under review) supported that LeIBP is structurally similar to the β-helical hyperactive AFPs [37,42,16]. Hence, we could speculate that

LeIBP may be hyperactive. LeIBP is, however, not hyperactive, which is supported by the fact that LeIBP does not have distinct conserved Thr-X-Thr motifs, arrays of which form IBS in the hyperactive AFPs. In our IBP structure instead, we identified a short array of Thr/Ser/Ala in one face of a three-faced β-helical structure, which is thought to be involved in binding to ice in the LeIBP's case. The ice morphology shape also confirmed this observation, as the burst pattern of ice crystal in the presence of LeIBP was not as explosive as other hyperactive AFPs [53,18,17]. Contrary to the low TH activity of LeIBP, recent characterization of AFPs from *F. cylindrus* and *T. ishikariensis* found that they have strong or hyper TH activities with a similar ice-binding pattern. With the limited data from the present study, it is hard to speculate why LeIBP is less active than other AFPs in the same class. Therefore, to better understand variations in TH activity and burst pattern, further structural and mutagenesis studies of this class of AFPs are needed.

Glycosylation is not essential for activity

The effect of N-linked glycosylation was evaluated with glycosylated (native LeIBP and pLeIBP) and non-glycosylated (HisbLeIBP) proteins. In LeIBP, glycosylation does not affect TH activity. This result is consistent with previous reports obtained with *Teneb-*

rio molitor, rainbow smelt, and carrot AFPs [60,1,11,40,25]. In the case of the *Solanum dulcamara* AFP, its non-glycosylated recombinant protein showed a lower activity than native AFP. Except for antifreeze glycoproteins [8], the glycan moiety is not directly involved in ice-binding. However, protein purification from a natural source could make the interpretation more or less complicated, as shown in our case. We noticed there was some discrepancy of TH activity between native and recombinant LeIBPs, regardless of glycosylation. This was probably due to the batch-to-batch variation in the native IBP sample preparation. In cold-finger ice affinity chromatography, some substances, for example polysaccharides, were carried over to the ice fraction and concentrated. These substances could not be removed completely and appeared to enhance the TH activity of native proteins (unpublished result). The recombinant LeIBPs, glycosylated or non-glycosylated, showed almost the same activity throughout the batches. These results, together with the finding that protease treatment completely abolished the activity of the native LeIBP sample [36], strongly suggest that the difference in TH activity between native and recombinant LeIBPs can be attributed to the enhancer inside the sample. Additionally, glycosylation of LeIBP did not affect the secondary and tertiary structures, the dimerization, nor the ice-binding preference. Therefore, the glycosylation may be important for *in vivo* protein folding and quality control [51].

To provide more insight on this class of AFPs or IBPs, we will focus on a few questions raised in this study. These include whether reversible dimerization or oligomerization is common in this class, and whether dimer formation increases or decreases the effective concentration of IBS. In addition, we will examine what causes the differences in TH activity and what faces or residues are involved in ice-binding.

Acknowledgements

References

[1] J.C. Achenbach, K.V. Ewart, Structural and functional characterization of a C type lectin like antifreeze protein from rainbow smelt (*Osmerus mordax*), Eur. J. Biochem. 269 (2002) 1219–1226.

[2] J.C. Achenbach, K.V. Ewart, Structural and functional characterization of a C-type lectin-like antifreeze protein from rainbow smelt (*Osmerus mordax*), Eur. J. Biochem. 269 (2002) 1219–1226.

[3] A.A. Antson, D.J. Smith, D.I. Roper, S. Lewis, L.S. Caves, C.S. Verma, S.L. Buckley, P.J. Lillford, R.E. Hubbard, Understanding the mechanism of ice binding by type III antifreeze proteins, J. Mol. Biol. 305 (2001) 875–889.

[4] M. Bayer-Giraldi, C. Uhlig, U. John, T. Mock, K. Valentin, Antifreeze proteins in polar sea ice diatoms: diversity and gene expression in the genus *Fragilariopsis*, Environ. Microbiol. 12 (2010) 1041–1052.

[5] M. Bayer-Giraldi, I. Weikusat, H. Besir, G. Dieckmann, Characterization of an antifreeze protein from the polar diatom *Fragilariopsis cylindrus* and its relevance in sea ice, Cryobiology 63 (2011) 210–219.

[6] G. Bohm, R. Muhr, R. Jaenicke, Quantitative analysis of protein far UV circular dichroism spectra by neural networks, Protein Eng. 5 (1992) 191–195.

[7] C.I. DeLuca, R. Comley, P.L. Davies, Antifreeze proteins bind independently to ice, Biophys. J. 74 (1998) 1502–1508.

[8] A.L. Devries, Glycoproteins as biological antifreeze agents in Antarctic fishes, Science 172 (1971) 1152.

[9] A.L. DeVries, Antifreeze glycopeptides and peptides: interactions with ice and water, Methods Enzymol. 127 (1986) 293–303.

[10] D. Doucet, M.G. Tyshenko, P.L. Davies, V.K. Walker, A family of expressed antifreeze protein genes from the moth, *Choristoneura fumiferana*, Eur. J. Biochem. 269 (2002) 38–46.

[11] J.G. Duman, Purification and characterization of a thermal hysteresis protein from a plant, the bittersweet nightshade *Solanum dulcamara*, Biochim. Biophys. Acta 1206 (1994) 129–135.

[12] J.G. Duman, T.M. Olsen, Thermal hysteresis protein activity in bacteria, fungi, and phylogenetically diverse plants, Cryobiology 30 (1993) 322–328.

[13] J.G. Duman, V. Bennett, T. Sformo, R. Hochstrasser, B.M. Barnes, Antifreeze proteins in Alaskan insects and spiders, J. Insect Physiol. 50 (2004) 259–266.

[14] K.V. Ewart, Q. Lin, C.L. Hew, Structure, function and evolution of antifreeze proteins, Cell. Mol. Life Sci. 55 (1999) 271–283.

[15] G.L. Fletcher, C.L. Hew, P.L. Davies, Antifreeze proteins of teleost fishes, Annu. Rev. Physiol. 63 (2001) 359–390.

[16] C.P. Garnham, J.A. Gilbert, C.P. Hartman, R.L. Campbell, J. Laybourn-Parry, P.L. Davies, A Ca2+-dependent bacterial antifreeze protein domain has a novel β-helical ice-binding fold, Biochem. J. 411 (2008) 171–180.

[17] J.A. Gilbert, P.L. Davies, J. Laybourn-Parry, A hyperactive, Ca2+-dependent antifreeze protein in an Antarctic bacterium, FEMS Microbiol. Lett. 245 (2005) 67–72.

[18] S.P. Graether, M.J. Kuiper, S.M. Gagne, V.K. Walker, Z. Jia, B.D. Sykes, P.L. Davies, β-helix structure and ice-binding properties of a hyperactive antifreeze protein from an insect, Nature 406 (2000) 325–328.

[19] L.A. Graham, P.L. Davies, Glycine-rich antifreeze proteins from snow fleas, Science 310 (2005) 461.

[20] L.A. Graham, Y.C. Liou, V.K. Walker, P.L. Davies, Hyperactive antifreeze protein from beetles, Nature 388 (1997) 727–728.

[21] L.A. Graham, C.B. Marshall, F.H. Lin, R.L. Campbell, P.L. Davies, Hyperactive antifreeze protein from fish contains multiple ice-binding sites, Biochemistry 47 (2008) 2051–2063.

[22] M. Griffith, M.W. Yaish, Antifreeze proteins in overwintering plants: a tale of two activities, Trends Plant Sci. 9 (2004) 399–405.

[23] M. Griffith, P. Ala, D.S. Yang, W.C. Hon, B.A. Moffatt, Antifreeze protein produced endogenously in winter rye leaves, Plant Physiol. 100 (1992) 593–596.

[24] T. Hoshino, M. Kiriaki, S. Ohgiya, M. Fujiwara, H. Kondo, Y. Nishimiya, I. Yumoto, S. Tsuda, Antifreeze proteins from snow mold fungi, Can. J. Bot. 81 (2003) 1175–1181.

[25] T. Huang, J. Nicodemus, D.G. Zarka, M.F. Thomashow, M. Wisniewski, J.G. Duman, Expression of an insect (*Dendroides canadensis*) antifreeze protein in *Arabidopsis thaliana* results in a decrease in plant freezing temperature, Plant Mol. Biol. 50 (2002) 333–344.

[26] M. Janech, A. Krell, T. Mock, J.-S. Kang, J.A. Raymond, Ice-binding proteins from sea ice diatoms (bacillariophyceae), J. Phycol. 42 (2006) 410–416.

[27] Z. Jia, P.L. Davies, Antifreeze proteins: an unusual receptor-ligand interaction, Trends Biochem. Sci. 27 (2002) 101–106.

[28] H. Kawahara, Y. Nakano, K. Omiya, N. Muryoi, J. Nishikawa, H. Obata, Production of two types of ice crystal-controlling proteins in Antarctic bacterium, J. Biosci. Bioeng. 98 (2004) 220–223.

[29] H. Kawahara, Y. Iwanaka, S. Higa, N. Muryoi, M. Sato, M. Honda, H. Omura, H. Obata, A novel, intracellular antifreeze protein in an antarctic bacterium, *Flavobacterium xanthum*, Cryo Lett. 28 (2007) 39–49.

[30] C.A. Knight, C.C. Cheng, A.L. DeVries, Adsorption of α-helical antifreeze peptides on specific ice crystal surface planes, Biophys. J. 59 (1991) 409–418.

[31] G.D. Knott, Comput. Programs Biomed. 10 (1979) 271–280.

[32] A. Krell, B. Beszteri, G. Dieckmann, G. Glöckner, K. Valentin, T. Mock, A new class of ice-binding proteins discovered in a salt-stress-induced cDNA library of the psychrophilic diatom *Fragilariopsis cylindrus* (Bacillariophyceae), Eur. J. Phycol. 43 (2008) 423–433.

[33] M.J. Kuiper, C. Lankin, S.Y. Gauthier, V.K. Walker, P.L. Davies, Purification of antifreeze proteins by adsorption to ice, Biochem. Biophys. Res. Commun. 300 (2003) 645–648.

[34] U.K. Laemmli, Cleavage of structural proteins during the assembly of the head of bacteriophage T4, Nature 227 (1970) 680–685.

[35] T.M. Laue, B.D. Shah, T.M. Ridgeway, S.L. Pelletier, Computer-aided interpretation of analytical sedimentation data for proteins, in: S.E. Harding et al. (Eds.), Analytical ultracentrifugation in biochemistry and polymer science, 1992, pp. 90–125.

[36] J.K. Lee, K.S. Park, S. Park, H. Park, Y.H. Song, S.H. Kang, H.J. Kim, An extracellular ice-binding glycoprotein from an Arctic psychrophilic yeast, Cryobiology 60 (2010) 222–228.

[37] E.K. Leinala, P.L. Davies, Z. Jia, Crystal structure of β-helical antifreeze protein points to a general ice binding model, Structure 10 (2002) 619–627.

[38] Z. Li, F. Xiong, Q. Lin, M. d'Anjou, A.J. Daugulis, D.S. Yang, C.L. Hew, Low-temperature increases the yield of biologically active herring antifreeze protein in *Pichia pastoris*, Protein Exp. Purif. 21 (2001) 438–445.

[39] F.H. Lin, P.L. Davies, L.A. Graham, The Thr- and Ala-rich hyperactive antifreeze protein from inchworm folds as a flat silk-like β-helix, Biochemistry 50 (2011) 4467–4478.

[40] Y.C. Liou, P. Thibault, V.K. Walker, P.L. Davies, L.A. Graham, A complex family of highly heterogeneous and internally repetitive hyperactive antifreeze proteins from the beetle *Tenebrio molitor*, Biochemistry 38 (1999) 11415–11424.

[41] X. Mao, Z. Liu, J. Ma, H. Pang, F. Zhang, Characterization of a novel β-helix antifreeze protein from the desert beetle *Anatolica polita*, Cryobiology 62 (2011) 91–99.

[42] C.B. Marshall, M.E. Daley, L.A. Graham, B.D. Sykes, P.L. Davies, Identification of the ice-binding face of antifreeze protein from *Tenebrio molitor*, FEBS Lett. 529 (2002) 261–267.

[43] C.B. Marshall, A. Chakrabartty, P.L. Davies, Hyperactive antifreeze protein from winter flounder is a very long rod-like dimer of β-helices, J. Biol. Chem. 280 (2005) 17920.

[44] C.B. Marshall, A. Chakrabartty, P.L. Davies, Hyperactive antifreeze protein from winter flounder is a very long rod-like dimer of α-helices, J. Biol. Chem. 280 (2005) 17920–17929.

[45] Y.F. Mok, F.H. Lin, L.A. Graham, Y. Celik, I. Braslavsky, P.L. Davies, Structural basis for the superior activity of the large isoform of snow flea antifreeze protein, Biochemistry 49 (2010) 2593–2603.

[46] A.K. Park, K.S. Park, H.J. Kim, H. Park, I.Y. Ahn, Y.M. Chi, J.H. Moon, Crystallization and preliminary X-ray crystallographic studies of the ice-binding protein from the Antarctic yeast *Leucosporidium* sp. AY30, Acta Cryst. F67 (2011) 800–802.

[47] J.A. Raymond, M.G. Janech, Ice-binding proteins from enoki and shiitake mushrooms, Cryobiology 58 (2009) 151–156.

[48] J.A. Raymond, C. Fritsen, K. Shen, An ice-binding protein from an Antarctic sea ice bacterium, FEMS Microbiol. Ecol. 61 (2007) 214–221.

[49] J.A. Raymond, B.C. Christner, S.C. Schuster, A bacterial ice-binding protein from the Vostok ice core, Extremophiles 12 (2008) 713–717.

[50] J.A. Raymond, M. Janech, C. Fritsen, Novel ice-binding proteins from a psychrophilic antarctic alga (chlamydomonadaceae, chlorophyceae), J. Phycol. 45 (2009) 130–136.

[51] J. Roth, C. Zuber, S. Park, I. Jang, Y. Lee, K.G. Kysela, V.L. Fourn, R. Santimaria, B. Guhl, J.W. Cho, Protein N-glycosylation, protein folding, and protein quality control, Mol. Cells 30 (2010) 497–506.

[52] J. Sambrook, E.F. Fritsch, T. Maniatis, Molecular Cloning: A Laboratory Manual, 1989.

[53] A.J. Scotter, C.B. Marshall, L.A. Graham, J.A. Gilbert, C.P. Garnham, P.L. Davies, The basis for hyperactivity of antifreeze proteins, Cryobiology 53 (2006) 229–239.

[54] M. Smallwood, D. Worrall, L. Byass, L. Elias, D. Ashford, C.J. Doucet, C. Holt, J. Telford, P. Lillford, D.J. Bowles, Isolation and characterization of a novel antifreeze protein from carrot (*Daucus carota*), Biochem. J. 340 (1999) 385–391.

[55] A.P. Tomchaney, J.P. Morris, S.H. Kang, J.G. Duman, Purification, composition, and physical properties of a thermal hysteresis "antifreeze" protein from larvae of the beetle, *Tenebrio molitor*, Biochemistry 21 (1982) 716–721.

[56] M.G. Tyshenko, D. Doucet, P.L. Davies, V.K. Walker, The antifreeze potential of the spruce budworm thermal hysteresis protein, Nat. Biotechnol. 15 (1997) 887–890.

[57] C. Uhlig, J. Kabisch, G.J. Palm, K. Valentin, T. Schweder, A. Krell, Heterologous expression, refolding and functional characterization of two antifreeze proteins from *Fragilariopsis cylindrus* (Bacillariophyceae), Cryobiology 63 (2011) 220–228.

[58] M.E. Urrutia, J.G. Duman, C.A. Knight, Plant thermal hysteresis proteins, Biochim. Biophys. Acta 1121 (1992) 199–206.

[59] X. Wang, A.L. DeVries, C.H. Cheng, Antifreeze peptide heterogeneity in an antarctic eel pout includes an unusually large major variant comprised of two 7 kDa type III AFPs linked in tandem, Biochim. Biophys. Acta 1247 (1995) 163–172.

[60] D. Worrall, L. Elias, D. Ashford, M. Smallwood, C. Sidebottom, P. Lillford, J. Telford, C. Holt, D. Bowles, A carrot leucine-rich-repeat protein that inhibits ice recrystallization, Science 282 (1998) 115.

[61] N. Xiao, K. Suzuki, Y. Nishimiya, H. Kondo, A. Miura, S. Tsuda, T. Hoshino, Comparison of functional properties of two fungal antifreeze proteins from *Antarctomyces psychrotrophicus* and *Typhula ishikariensis*, FEBS J. 277 (2010) 394–403.